Progress In Electromagnetics Research C, Vol. 101, 203–218, 2020

A Novel Complementary Slotted Split Ring Resonator Loaded Truncated Arc Patch Antenna with Enhanced Performance

Maroli S. Rao* **and Prabhugoud I. Basarkod**

Abstract—This paper proposes a truncated arc patch antenna loaded with a novel complementary slotted split ring resonator (CSlSRR) in the ground plane. The antenna achieves wide bandwidth, circular polarisation (CP), and omnidirectional radiation pattern in the S-band. The electrical size of the antenna is $0.36\lambda_0 \times 0.31\lambda_0$, and the radiating metal dimension is $0.18\lambda_0 \times 0.21\lambda_0$ (λ_0 corresponds to $f_0 = 2.45\,\text{GHz}$). Truncated corners with a semi-circular arc produce CP with the inset feed. The CSlSRR helps in improving the bandwidth and miniaturisation of the antenna. The design achieves a size reduction of 61%. The fabricated antenna exhibits 12.3% impedance bandwidth (IBW), 4.07% axial ratio bandwidth (ARBW), and a maximum gain of 2.476 dBi at 2.75 GHz. The antenna prototype is characterised in an anechoic chamber. The paper carries out a comparison of the measured and simulated results and other reported works in literature.

1. INTRODUCTION

Design and implementation of electrically small antennas for various wireless applications and standards are the need of the hour. Microstrip patch antennas have the advantage of being planar, low profile, and being easily integrable with modern-day monolithic integrated circuits. Hence, the increased use of patch antennas is in many devices in domestic, medical, industrial, aeronautical, and space applications. A simple patch antenna also comes accompanied with limitations like low bandwidth, limited gain, and linear polarisation. Efforts to improve these parameters have always been the endeavour of the researchers working in this field. Several techniques have evolved awhile to enhance the performance of a patch antenna to make it more attractive and adaptive for various applications and domains. A few of the methods employed are — use of high dielectric value substrates for miniaturisation, use of defective or partial grounds to improve bandwidths [1–4], use of superstrates to improve gain [5, 6], and employing unique structures like split ring resonators to enhance radiative gain and bandwidth [7–11].

Another feature which attracts many researchers is the design of circularly polarised patch antennas. CP antennas are capable of communicating irrespective of their alignment and have great advantage in moving platforms which exhibit orientation/attitude change. Patch antennas designed to produce CP exhibit poor axial ratio bandwidths (ARBW). Numerous methods are in fashion to improve the ARBW of patch antennas and make them more versatile. The most popular method of obtaining CP is by incorporating dual orthogonal feed to the radiating patch [12, 13]. The orthogonal feed can be designed by quadrature hybrid, ring hybrid, or Wilkinson power divider to name a few of the techniques.

The use of metamaterials has helped antenna designers in reducing the overall size of the antenna without overtly compromising the performance. Split ring resonators (SRR) have been embedded within the patch to improve the performance of patch antennas. In some cases, the structures are laid around the radiating patch to bring about improvements in the characteristics [9, 11]. Another popular configuration is the complementary split ring resonator (CSRR) etched into the ground plane of the

Received 10 March 2020, Accepted 26 April 2020, Scheduled 8 May 2020
* Corresponding author: Maroli Shailesh Rao (marolishaileshrao@hotmail.com).
The authors are with the School of Electronics and Communication Engineering, REVA University, Bengaluru 560064, India.

antenna [14, 15]. These complementary structures exhibit inverse properties of an SRR as verified by Babinet's principle. The CSRR aids in a further reduction in the size of the patch antenna and improving the impedance bandwidth (IBW) [16]. The cases using fractal trees in the ground plane have also been presented to design CP antenna in the 2.4 GHz ISM band [17]. The available literature also indicates different types of resonating structures etched on the surface to enhance the performance of the antenna [18, 19]. Utilising reactive impedance surfaces to improve bandwidth and produce CP is another option exercised by researchers [20].

Catano-Ochoa et al. discussed the use of an array of hexagonal CSRR on a simple rectangular patch antenna to reduce the resonance frequency and improve the impedance matching [21]. A printed compact monopole was presented utilising an SNG material with near-zero refractive index in [22]. The monopole antenna is UWB in nature and has a gain of 6.12 dBi. Al-Bawri et al. discussed a quadband antenna with a novel zero refractive index and DNG material with an enhanced gain of 6.74 dBi and IBW of 28% in [23]. A THz regime antenna was presented using a 3D MTM structure over a conventional patch to get a more focused main beam with an improved gain in [24]. Metamaterials aided in improving the overall performance of devices in biomedical and bioengineering domains operating in the THz frequency region [25, 26]. Metamaterial embedded devices were used as sensors to characterise the relative permittivity of various dielectric materials [27, 28]. CSRR used in obtaining high-quality factor structures for deployment in low phase noise oscillators, multi-band diplexers and filters shows its versatility [29]. MTM inspired UWB antenna in the radiating patch, as well as the ground plane with high gain, is reported in [30]. Chapter 4 of the book *Metamaterials and Metasurfaces* deals with applications of metamaterials in design to enhance the antenna parameters [31].

In this article, we discuss a simple rectangular patch antenna with truncated arced corners, fabricated on an FR4 substrate with a novel CSlSRR exhibiting negative material parameters. The patch is excited by an inset feed. The CSlSRR and the truncated arced corners facilitate the antenna in improving the bandwidth and generating CP. The antenna is suitable for the use in the WLAN (both licensed and unlicensed bands) and WiMAX applications. There are four sections in this paper. Section 2 deals with antenna design philosophy, parametric analysis, and CSlSRR unit cell deductions. Section 3 of the article discusses the results obtained through numerical/circuit analysis and measurement of the fabricated antenna. Finally, Section 4 forms the concluding part of the article.

2. TRUNCATED ARC PATCH ANTENNA, CSLSRR — DESIGN AND ANALYSIS

The material used for fabrication of the antenna is FR4 with a nominal thickness of 1.6 mm. The relative permittivity is 4.4, and loss tangent is 0.02. Ansys HFSS electromagnetic solver software is used for simulation of the various designs. Open source software Veusz is used for the graphical plotting of the results. Figure 1 depicts the physical dimensions and structural components of the antenna. The design uses inset feed to excite the patch. The dimension of the antenna is $44.6 \times 37.5 \times 1.6\,\text{mm}^3$. The radiating patch size is $22.3 \times 25\,\text{mm}^2$. Table 1 lists the various physical aspects of the optimised antenna.

Table 1. Optimised parameters of the proposed antenna (all values in mm).

Parameter	W_{sub}	L_{sub}	W_p	L_p	h	Fd_w	X_{fd}	y_0	w_1
Value	37.5	44.6	25	22.3	1.6	1.625	2.4375	3.7	1.65
Parameter	r_1	s	w_2	l_1	r_2	g_1	l_2	y_1	
Value	11	1.05	0.4	4.1	1.75	1.95	7.1	11.15	

The following subsections discuss the design methodology of the novel CSlSRR structure and the evolution stages of the truncated arc patch antenna.

2.1. Design of the Novel Complimentary Slotted Split Ring Resonator

In this section, we take the discussion of a novel complimentary slotted split ring resonator design. Figure 1(b) depicts the novel CSlSRR structure. The composition comprises two concentric slots with

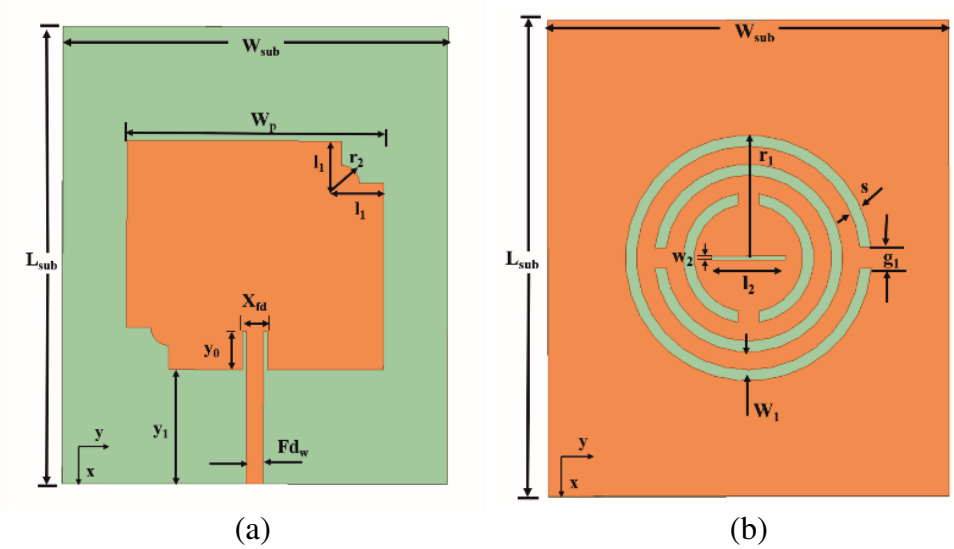

Figure 1. Image of the truncated arc patch antenna and the novel CSlSRR etched ground plane. (a) Top layer. (b) Bottom layer.

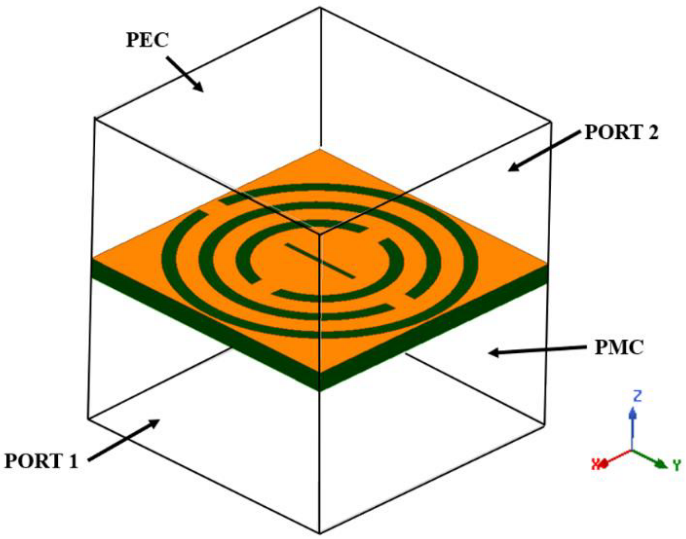

Figure 2. Unit cell set up for extraction of material parameters of the CSlSRR.

metal bridges on the opposite sides of the ring. The third ring bridge is placed perpendicular to the first two bridges and encloses a narrow linear groove in the centre. The slot is placed equidistant from the innermost circular slots. Table 1 lists the dimensions of the CSlSRR. Figure 2 depicts the setup of the CSlSRR unit cell for the extraction of the material parameters. The unit cell size is of $25.3 \times 25.3\,\text{mm}^2$. The port is excited along the x-axis. The planes along z-axis are defined to be perfect electric conductors (PEC), and the ones along the y-axis are defined as a perfect magnetic conductor (PMC). The CSlSRR responds to a perpendicular electric field travelling along the x-axis. Figure 3(a) shows the S-parameter response of the unit cell. The stopband of the cell occurs at 2.996 GHz. After obtaining the S-parameters from Ansys HFSS, the data file is processed in MATLAB to extract the material parameters of the structure.

A suitable method can be applied to extract parameters of the CSlSRR from the S-parameters [32–36]. In this article, we utilise Nicholson-Ross-Weir (NRW) technique for calculating the permeability, permittivity, and refractive index of the novel CSlSRR. Figure 3(b) illustrates the extracted parameters

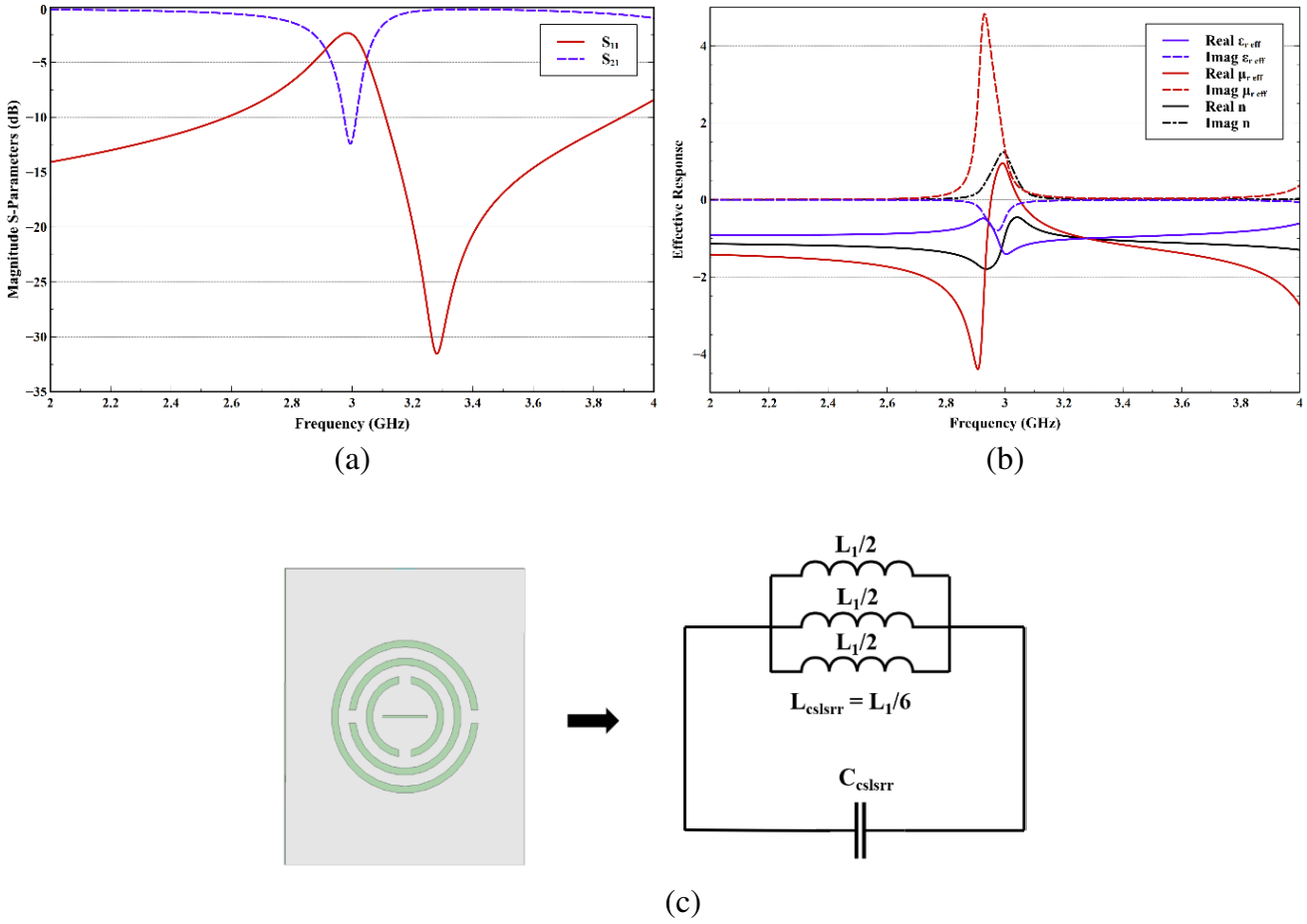

Figure 3. (a) S-parameter response of the novel CSlSRR unit cell. (b) Extracted material parameters. (c) CSlSRR equivalent lumped circuit representation.

of the resonant structure. The plot indicates a double negative (DNG) characteristics response to the novel CSlSRR design. The designs discussed in the literature have shown only single negative (SNG) responses for the models [18, 19]. In the proposed structure, the dual negative characteristic is obtained due to the centre slot in the CSRR structure which changes the course of currents from being circular to a linear flow in the centre portion of the CSlSRR. The annular rings produce opposing currents in the metal portion of the CSRR on either side of the slots. However, the current at the bridge of the innermost ring flows linearly across the narrow slot.

Analytically, the CSlSRR structure can be represented as a parallel combination of inductance and capacitance. In literature, there are different approaches for extracting the values of these elements based on either the transmission line model or quasi-static model [37, 38]. Figure 3(c) shows a simple lumped equivalent circuit model of the novel CSlSRR structure. L_{cslsrr} is the equivalent inductance, and C_{cslsrr} is the equivalent capacitance of the novel structure. The expression for resonating frequency of the structure is given in Eq. (1),

$$f_r = \frac{1}{2\Pi} \frac{1}{\sqrt{L_{\text{cslsrr}} C_{\text{cslsrr}}}} \tag{1}$$

2.2. Design Evolution of the Truncated Arc Patch Antenna

The design originated with the use of a transmission line model to arrive at the first form of the antenna as depicted in Figure 4(a). The transmission line model, as discussed in Chapter 14 of *Antenna Theory*

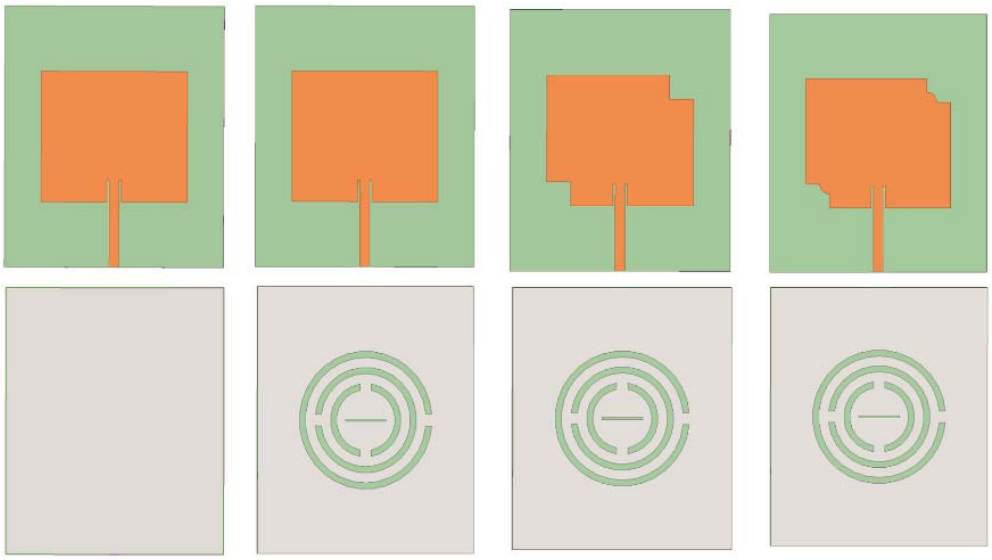

Figure 4. Evolution of the design from simple patch to final stage (a) Ant1, (b) Ant2, (c) Ant3 and (d) Ant4.

— *Analysis and Design* by Balanis [39], is the starting point for the physical dimensions of the antenna. The effective relative permittivity (ε_{reff}) of the antenna when the ratio $w/h > 1$ is given in Eq. (2),

$$\varepsilon_{reff} = \frac{\varepsilon_r + 1}{2} + \frac{\varepsilon_r - 1}{2}\left[1 + 12\frac{h}{w}\right]^{-1/2} \tag{2}$$

The width of the patch (W_p) is related to the resonant frequency (f_r), the velocity of light in free space (c), and relativity permittivity (ε_r) by the relationship in Eq. (3),

$$W_p = \frac{c}{2f_r}\sqrt{\frac{2}{\varepsilon_r + 1}} \tag{3}$$

Consider the dominant mode of excitation (TM_{100}) of the patch antenna, and the patch length is given by Eq. (4) as,

$$L_P = \frac{c}{2f_r\sqrt{\varepsilon_{reff}}} \tag{4}$$

The length and width of the patch are then iteratively fine-tuned to obtain the best response for the design. The design utilises inset feed to obtain wideband impedance matching. The calculation of the inset length (y_0) into the patch utilising the equation in Eq. (5),

$$R_{in(y=y_0)} = R_{in(y=0)}\mathrm{Cos}^2\left(\frac{\pi}{L_P}y_0\right) \tag{5}$$

where $R_{in(y=y_0)} = 50\,\Omega$ and $R_{in(y=0)}$ is the impedance at the edge of the patch. The dimension of the substrate length is taken as twice that of the patch length ($L_{sub} = 2L_p$) and the width as one and half times the patch width ($W_{sub} = 1.5W_p$).

The work aims to propose a simple, easy to fabricate, compact patch antenna with enhanced bandwidth, circular polarisation, and decent gain in the 2.4 to 2.7 GHz band of frequency utilised for WLAN and WiMAX applications. The design exercise began with the layout of a simple rectangular patch antenna Ant1, as shown in Figure 4(a). Ant1 resonates at 3.09 GHz and exhibits an impedance bandwidth (IBW) of 103 MHz (3.33%). The size of the patch is $22.5 \times 25\,\mathrm{mm}^2$. The substrate used is FR4 of thickness 1.6 mm. Figure 4(b) shows Ant2 with the novel CSlSRR etched in the ground plane of the antenna. Ant2 has a resonance frequency at 2.441 GHz and IBW of 223 MHz (9.17%).

Ant3 (Figure 4(c)) has the top right and bottom left corners truncated by equal lengths in both the x- and y-directions. The truncated antenna Ant3 resonates distinctly in two bands with a cut-off around 40 MHz between the two. In the first, resonance occurs at 2.44 GHz and extends from 2.38 to 2.49 GHz possessing an IBW of 4.5%. In the second, resonance occurs at 2.637 GHz, and the frequency range extends from 2.53 to 2.75 GHz (IBW of 8.3%). In the fourth stage, we introduce an arc in the truncated region with a radius of r_2. This arc brings about two changes in Ant4 (Figure 4(d)). Firstly, the antenna resonates with an enhanced bandwidth without any splits in the band of 2.39 GHz to 2.72 GHz (330 MHz). Secondly, there is an improvement in the reflection coefficient of the resonant frequencies indicating a better impedance match. Ant4 has dual resonances in the band at 2.45 GHz and 2.605 GHz with IBW of 12.9%.

The truncated patch antenna introduces circular polarisation for the radiation at 2.5 GHz. Figures 5(a), (b) show the reflection coefficient S_{11} and axial ratio of the antennas under various stages of the design evolution observed during the simulation. We can see that the arc in the final design brings about the right matching leading to better radiation characteristics of the patch antenna.

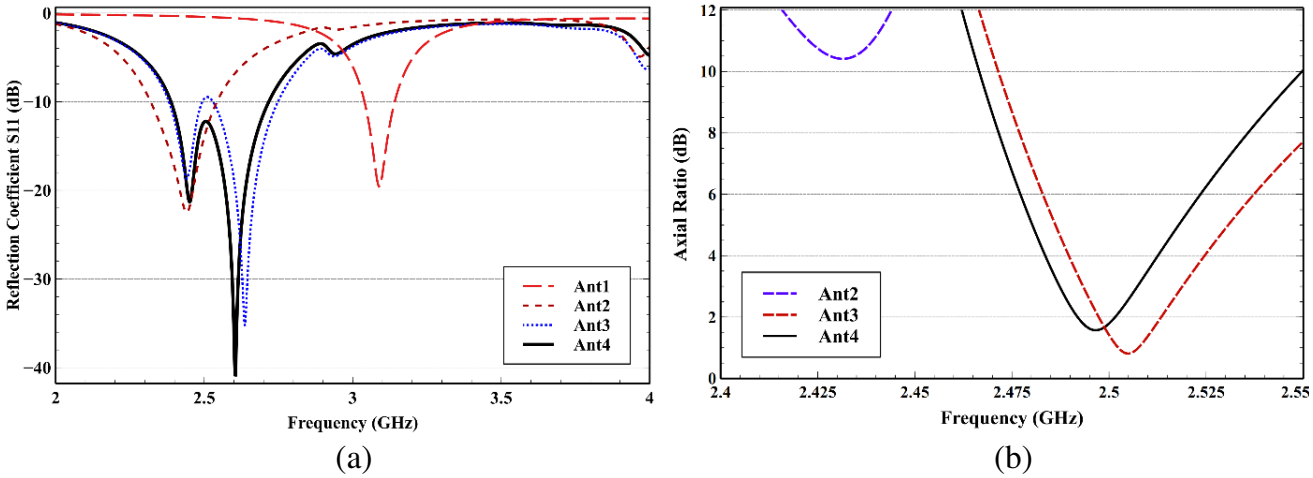

Figure 5. Results of the simulation of the antenna under various design evolution. (a) Reflection coefficient (S_{11}). (b) Axial ratio.

2.3. Study of Antenna Performance by Varying Structural Parameters

A detailed parametric analysis of the truncated arc patch antenna is carried out in this subsection to understand the impact of the change in parameters of the design on its performance. The critical responses of the antenna considered for comparison are the reflection coefficient and axial ratio of the antenna for parametric variations of the design values. The physical parameters selected are arc radius (r_2), the spacing gap of the split rings (s), and the ring width of the novel CSlSRR metallisation (w_1).

Figure 6 illustrates the effect of change of r_2 on reflection coefficient S_{11} and axial ratio. When a value of $r_2 = 1.75$ mm is used, the matching at both the resonant frequencies is perfect, and the axial ratio is also well below 3 dB. The axial ratio with $r_2 = 1.65$ mm is better, but the reflection coefficient at 2.5 GHz is close to −10 dB, which is not a comfortable situation considering fabrication and measurement errors which may creep into a prototype. The variation of the spacing between the rings or slot width s of the novel CSlSRR is another new study for performance of the antenna. The S_{11} graph in Figure 7(a) shows that with the reduction in s (to 1.0 mm), the dual resonances disappear, and the IBW also decreases. For $s = 1.05$ or 1.1 mm, the antenna exhibits dual resonances and improved IBW. However, the value of 1.05 mm is found more suitable due to better impedance matching. Glancing at the AR graph in Figure 7(b) indicates the extensive displacement of the AR response for the small changes in the dimension of s. It is an encouraging result for the study of the feasibility of utilising this aspect for obtaining varying AR bands as future work. As the focus of our current research is on getting circular polarisation at 2.5 GHz, we choose a value of 1.05 mm for s.

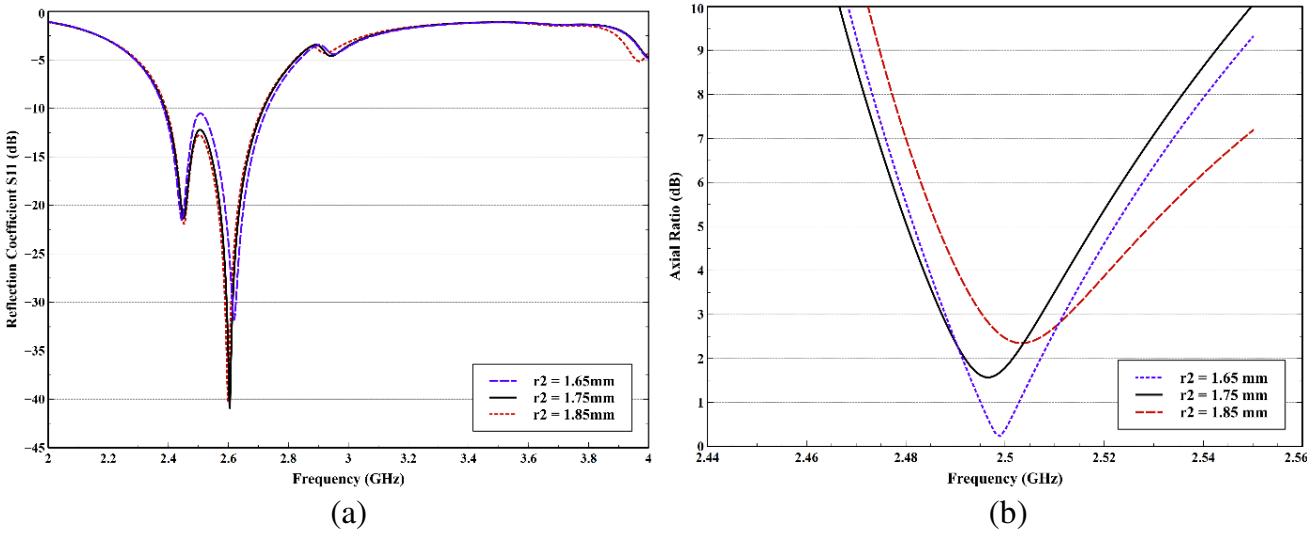

Figure 6. Impact of variation of patch arc radius r_2. (a) Reflection coefficient (S_{11}). (b) Axial ratio.

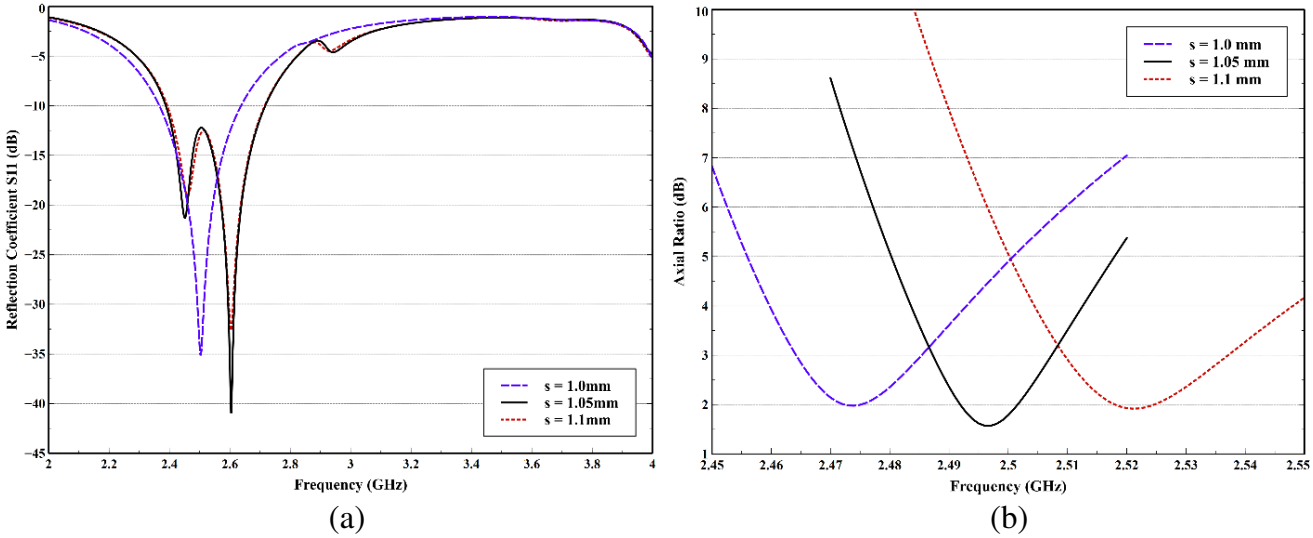

Figure 7. Impact of variation of slot width s. (a) Reflection coefficient (S_{11}). (b) Axial ratio.

The third parameter taken up for study is the ring width w_1 of CSlSRR. The width of the metallisation impacts the overall inductance of the complementary resonating structure. The impact of the change of the slot width w_1 is predominantly seen in the axial ratio, as observed in Figure 8(b). The AR position shifts to the mid 2.5–2.6 GHz with the increase in the gap distance. We choose a value of 1.65 mm as it is apt for 3 dB AR centred at 2.5 GHz. Figure 8(a) depicts the S_{11} results for the various values do not show much of a difference in all the three cases (better impedance matching at 2.6 GHz for $w_1 = 1.65$ mm).

3. FABRICATION OF TRUNCATED ARC ANTENNA, MEASUREMENTS AND DISCUSSIONS

The manufacture of the proposed design is carried out by the photolithographic method on an FR4 substrate. Figure 9 shows the image of the fabricated antenna's radiating patch and the ground plane

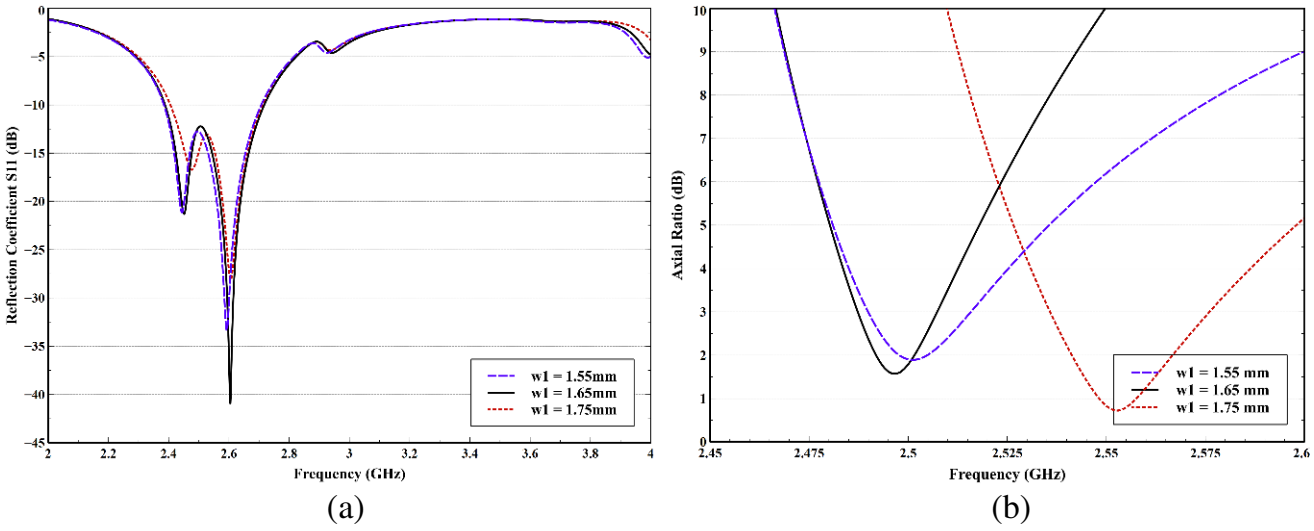

Figure 8. Impact of variation of slot width w_1. (a) Reflection coefficient (S_{11}). (b) Axial ratio.

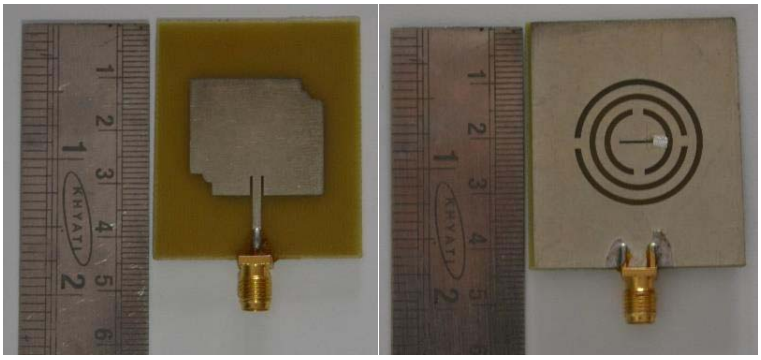

Figure 9. Images of the fabricated truncated arc antenna top layer and ground plane with the novel CSlSRR.

with the novel CSlSRR. The proposed antenna's electrical dimension is $0.36\lambda_0 \times 0.31\lambda_0 \times 0.013\lambda_0$, and the patch dimension is of the order of $0.18\lambda_0 \times 0.21\lambda_0 \times 0.013\lambda_0$ calculated at the first resonance frequency of 2.45 GHz. A miniaturisation level of approximately 61% is obtained in the antenna patch size compared to a conventional design.

Now let us consider the reflection coefficient of the proposed design. The reflection coefficient of the fabricated prototype is measured using Anritsu Site Master S820E VNA. Figure 10(a) shows the reflection coefficient S_{11} plotted against the frequency for three cases. The first case is that of numerical analysis; the second is that of circuit simulation; and the third is the measured result of the fabricated prototype. Figure 10(a) shows a good match between the numerical and circuit analysis responses of the proposed design. The response of the fabricated antenna matches with the other two responses but shows a shift around 30 MHz in the first resonant frequency. Due care was taken during the fabrication of antenna by ensuring adequate quality control measures (antenna fabrication done by a firm specializing in its manufacture). The factors like fabrication tolerance and measurement errors which inadvertently creeps in during the process contribute to the errors. The reflection coefficient of the fabricated prototype indicates a good response (< -10 dB) between 2.44 and 2.76 GHz producing an IBW of 320 MHz which is comparable to the simulation results.

Figure 10(b) shows the equivalent circuit of the proposed patch antenna. The circuit analysis is carried out using Keysight ADS. The values of the lumped components are $L_P = 4.5$ nH, $C_C = 0.430757$ pF, $L_{\mathrm{SRR1}} = 0.015$ nH, $C_{\mathrm{SRR1}} = 243$ pF, $L_{\mathrm{SRR2}} = 0.3506$ nH, $C_{\mathrm{SRR2}} = 46.5$ pF,

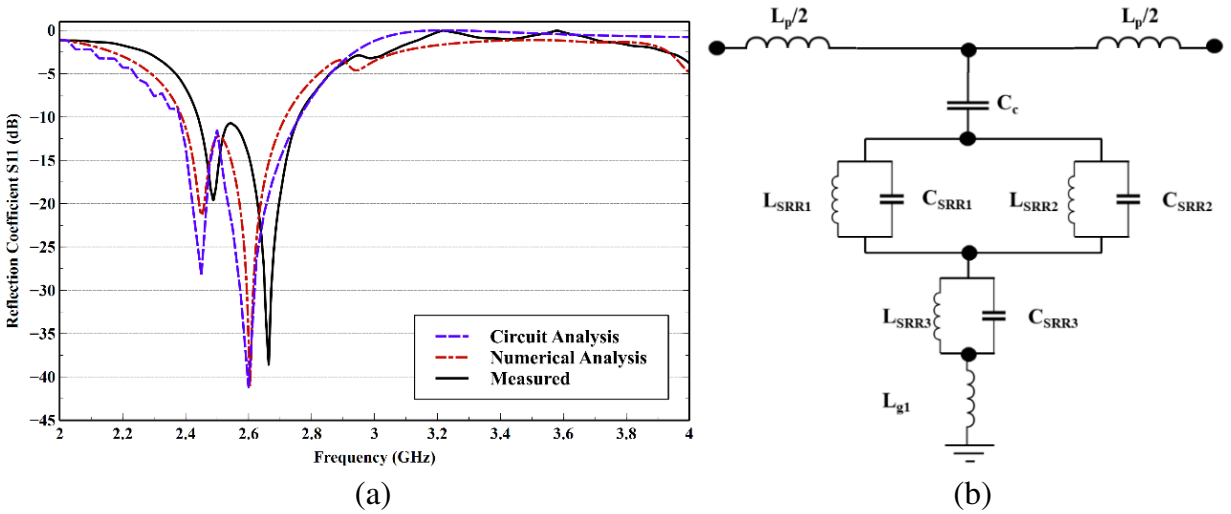

Figure 10. (a) The reflection coefficient S_{11} of the proposed design for the three cases. (b) Equivalent circuit of the proposed patch antenna.

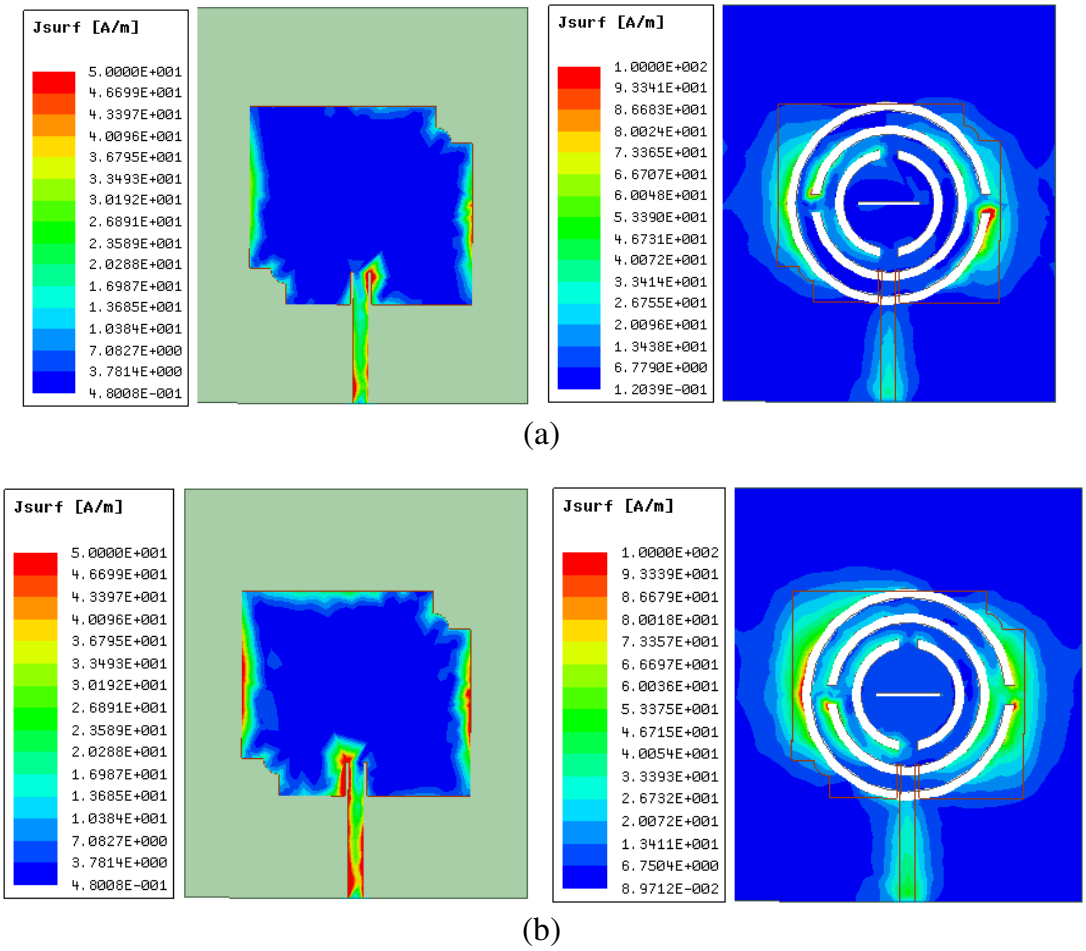

Figure 11. Distribution of current on the patch and ground plane (a) 2.5 GHz, (b) 2.66 GHz.

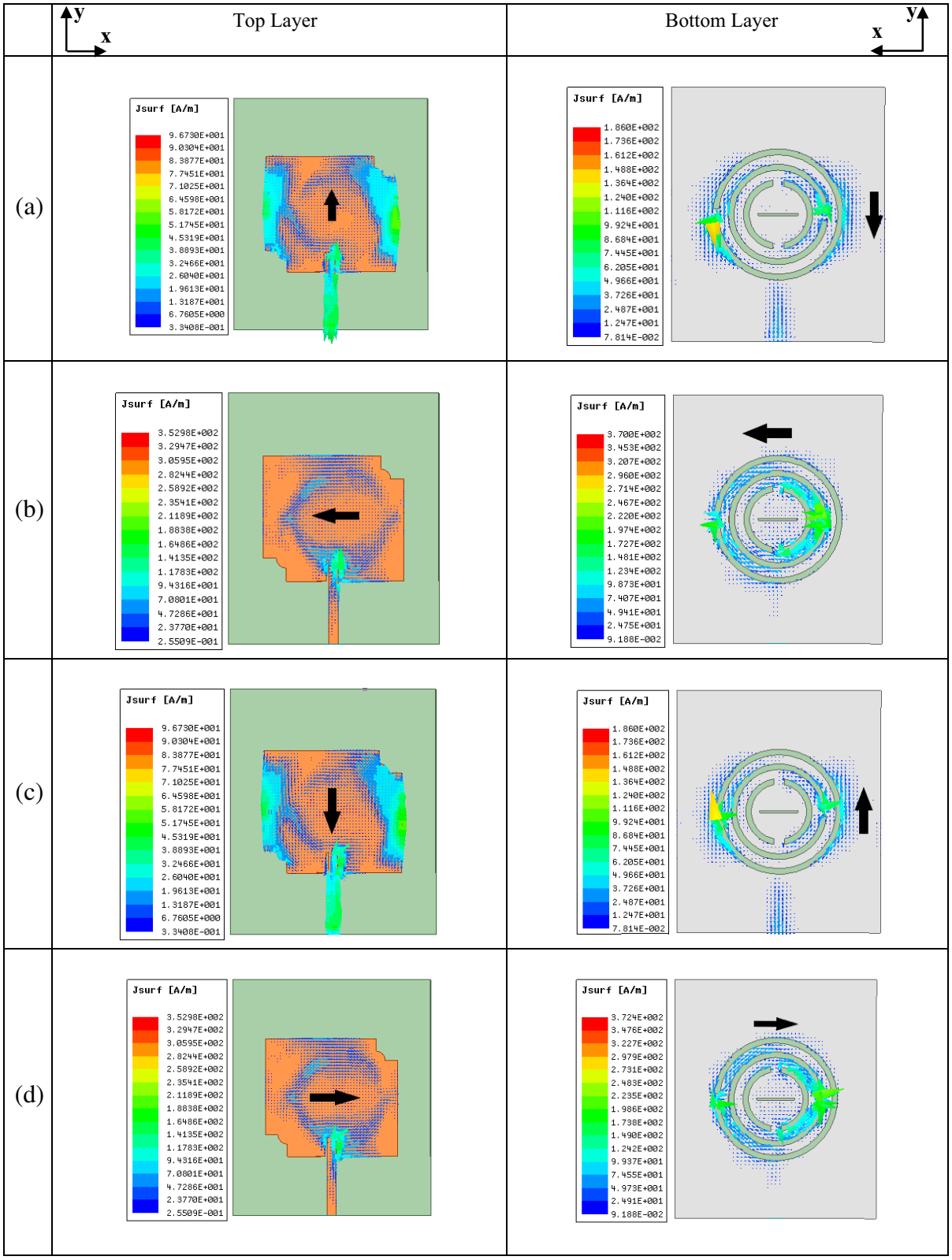

Figure 12. Vector current distribution on top and bottom surfaces of the proposed antenna at 2.5 GHz indicating RHCP (a) 0 deg, (b) 90 deg, (c) 180 deg, (d) 270 deg.

$L_{SRR3} = 0.05$ nH, $C_{SRR3} = 12$ pF and $L_{g1} = 5.63$ nH.

The patch and the novel CSlSRR structure resonate in tandem when being excited by EM wave to produce dual resonances in the band 2.4–2.7 GHz. The resonance nature is akin to a response by the long and short arms of a dipole antenna. The truncated corners produce circular polarisation due to inducement of orthogonal modes. Figures 11(a), (b) show the excitation of currents at 2.5 GHz and 2.66 GHz on the patch and ground plane, respectively. We observe from the figure that the patch and ground plane are identically excited in amplitude at both the resonant frequencies.

The plot of the vector current distribution on the patch confirms the type of polarisation emitted by the patch antenna. Figure 12 shows the vector current distribution of the antenna at 2.5 GHz. We note from the figure that the sense of direction of current flow for the various phase angles indicates an anti-clockwise movement. It shows right hand circularly polarised radiation characteristics of the truncated arc patch antenna. An alternative approach to determine the sense of polarisation could be utilising the polarisation ratio of RH and LH components and plotting it along with the phase angle change at the point where circular polarisation is present.

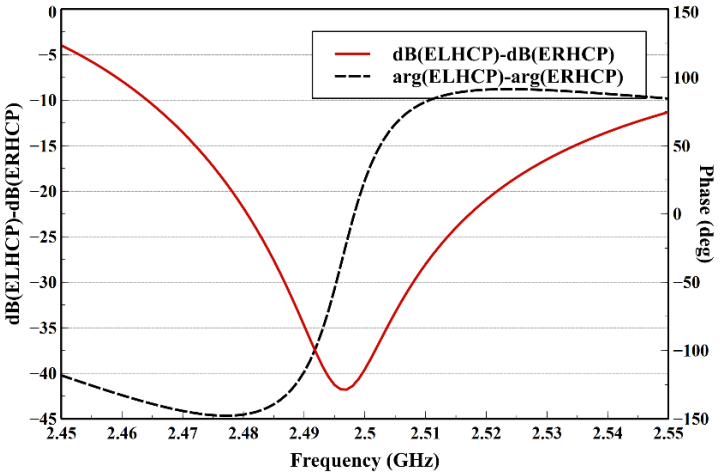

Figure 13. Polarisation amplitude and phase of the proposed antenna indicating RHCP at 2.5 GHz.

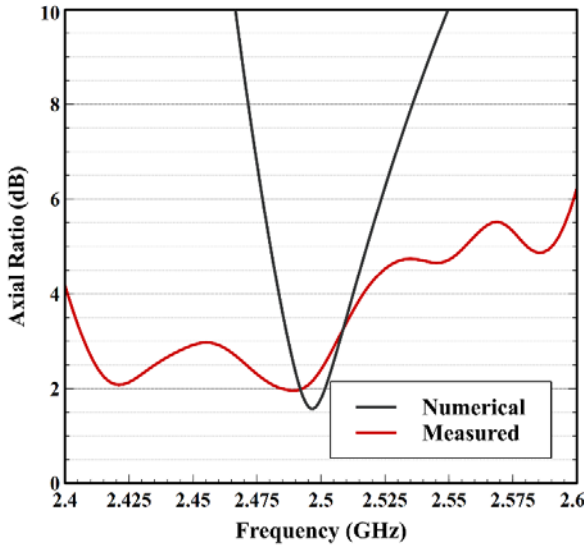

Figure 14. The measured and simulated axial ratio of the proposed truncated arc patch antenna with novel CSlSRR.

Figure 13 shows a plot of the difference between RH and LH polarisation amplitudes (in dB) co-plotted with the phase change. The plot shows a clear-cut negative value for the magnitude and a phase changing from negative to positive at the point where the circular polarisation is present. It indicates the right-handed nature of propagation of the EM waves emitted by the antenna. If the antenna had left-handed characteristics, then, the amplitude difference would have been positive, and the phase angle would have changed from positive to negative.

The fabricated antenna is put in an anechoic chamber to measure the various radiation characteristics. Figure 14 shows the measured and simulated axial ratios of the antenna. The measured axial ratio bandwidth of the antenna is 100 MHz (2.407 to 2.507 GHz), and the simulated AR is 20 MHz

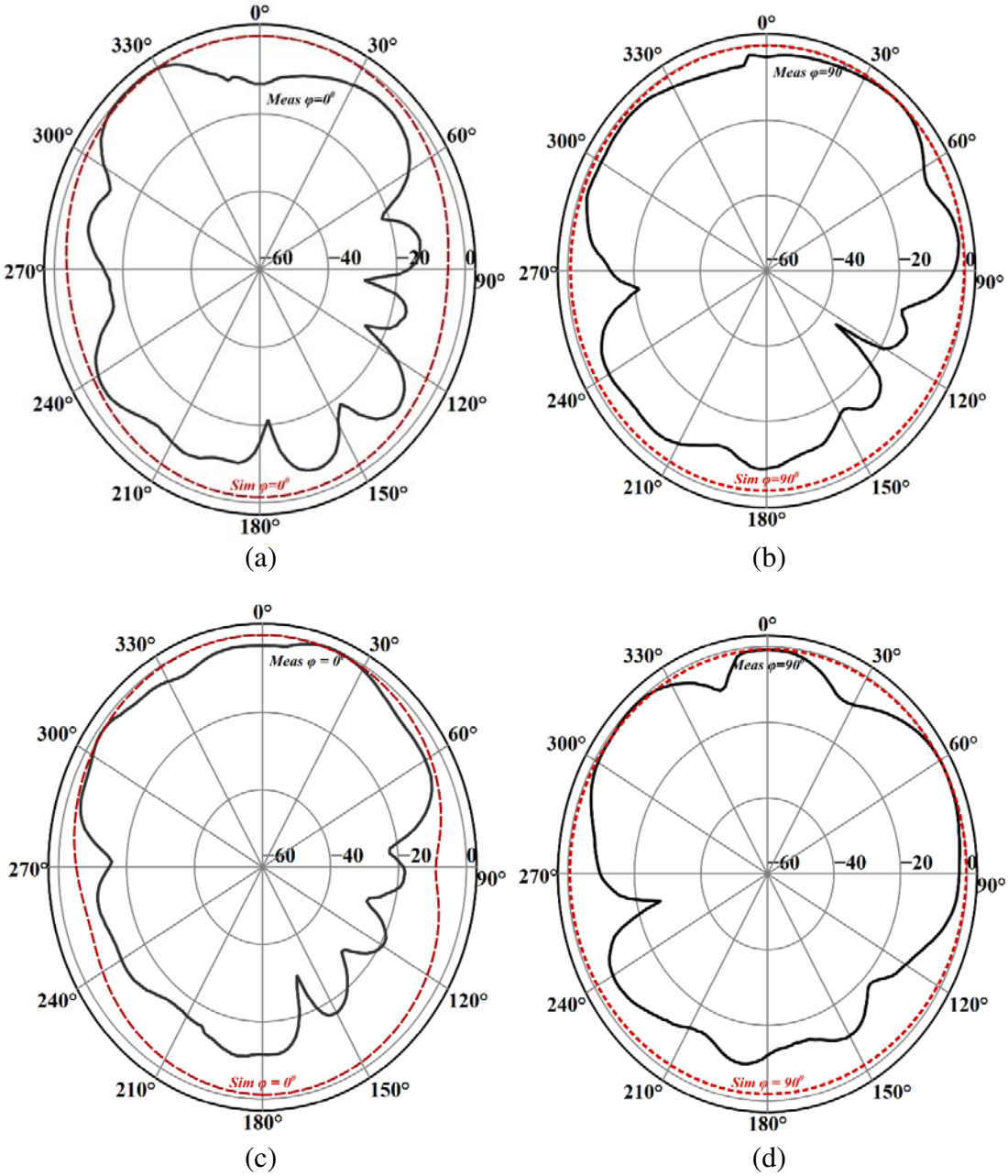

Figure 15. Normalised simulated and measured radiation pattern of the proposed antenna (a) E-plane 2.48 GHz, (b) H-plane 2.48 GHz, (c) E-plane 2.66 GHz, (d) H-plane 2.66 GHz.

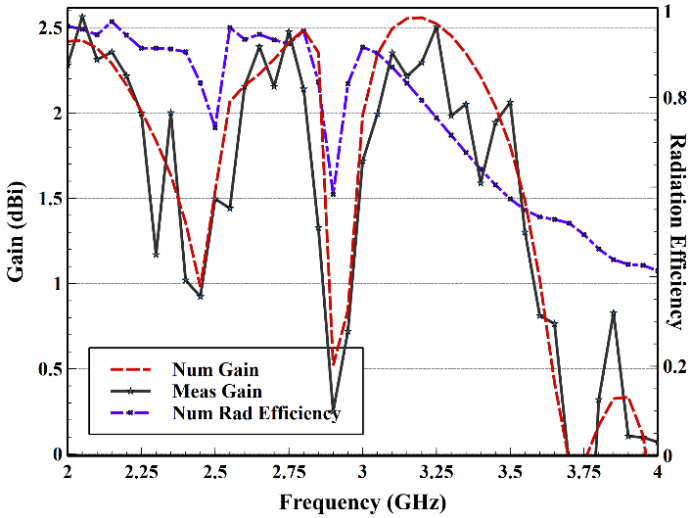

Figure 16. Gain & radiation efficiency of the proposed design (numerical and measured values).

Table 2. Comparison between the proposed antenna and other compact antennas reported in the literature.

Ref	Res Freq (GHz)	Antenna Size	Patch Size	Max Gain (dB)	IBW (%)	ARBW (%)	Structure Type	Polarisation
G. Singh et al. [16]	2.48, 3.16	30×35 mm^2	18.6×20 mm^2	1.09	6.04, 1.94	< 1	D-shaped CSRR	CP, LP
Parvathy et al. [12]	2.45	60×42 mm^2	50×25 mm^2	3.8	10.48	18.55	Square SRR	CP
S. K. Pandey et al. [17]	2.40	62×62 mm^2	28×28 mm^2	4.62	4.52	1.08	Modified FTDGS	CP
M. Jafar et al. [13]	2.05	105×105 mm^2	$R = 38$ mm	1.149	38.23	22.8	Slit on patch	CP
G. Samanta et al. [20]	3.7	40×40 mm^2	Side length $= 10$ mm	3.24	9.89	2.3	Hexa-RIS	CP
D. Catano-Ochoa et al. [21]	1.997	67×54	34.3×44.2	-	-	-	Hexagonal CSRR	LP
S. S. Al-Bawri et al. [22]	UWB (3.08–14.1)	22.5×14	$\Phi = 6$ mm	6.12	128.3	NA	NZRI/SNG MTM	LP
S. S. Al-Bawri et al. [23]	0.9, 2.4, 3.5, 5.5	78.6×42.5	-	6.72	28	NA	NZRI & DNG MTM	LP
A. A. A. Abdelrehim et al. [24]	10, 303	5.6×11.8	-	8	-	-	3D MTM	LP
H. Umair et al. [30]	UWB (4–16)	30.4×27	16×12	8.2	120	NA	Star-Shape & Square Shaped Crossed Slots	LP
Proposed	**2.48, 2.66**	**44.6×37.5 mm^2**	**22.3×25 mm^2**	**2.476**	**12.9**	**4.07**	**Novel CSlSRR**	**CP, LP**

(0.8% ARBW). The measured ARBW translates to 4.07%.

The radiation measurement is done in an anechoic chamber of dimension $7 \times 4 \times 3\,m^3$. The separation between the antenna under test (AUT) and the source antenna is 5.5 m within the chamber. The AUT is mounted on a pedestal having rotation capability in all the three axes. The source antenna is a calibrated broadband horn antenna with linear polarisation with a gain of 10 dB. Figures 15(a) to (d) indicate the radiation pattern of the proposed antenna in the E- and H-planes at 2.48 GHz and 2.66 GHz, the two resonant frequency points of the fabricated prototype. The radiation pattern is omnidirectional. We note that there is a perfect match between the simulated and measured radiation patterns. The kinks observed in the measured pattern are due to certain limitations in the anechoic chamber (interference due to servo motor mounts, leading to variation in power level readings).

Figure 16 shows the gain and radiation efficiency response of the proposed antenna. The antenna has simulated gains of 0.979 dBi and 2.412 dBi at 2.45 and 2.75 GHz, respectively, while the measured gains at the given frequencies are 0.923 dBi and 2.476 dBi, respectively. The radiation efficiency of the antenna is greater than 70% in the response band of the antenna. The maximum radiation efficiency obtained is 96% at 2.55 GHz, indicating high efficiency in the desired band of frequencies.

Table 2 is the summary of the performance of the proposed truncated arc patch antenna design with novel CSlSRR with other models reported in the literature. The proposed design has excellent bandwidth both in terms of impedance and axial ratios. The peak gain is also comparable to the results achieved by other researchers. The design also achieves proper miniaturisation levels too.

4. CONCLUSION

This research article has successfully proposed a truncated arc patch antenna with a novel complementary slotted split ring resonator in the ground plane. The paper has discussed the design from the perspective of numerical and circuit theory aspect and the results subsequently compared with the measured values. We have conducted a detailed parametric analysis to ascertain the values of the design parameters of the patch and the novel CSlSRR. The fabricated antenna resonates at 2.48 GHz and 2.66 GHz in the band of 2.44 to 2.76 GHz. The measured contiguous impedance bandwidth is 320 MHz (12.3%). RHCP is generated along the boresight and has a 100 MHz (4.07%) axial ratio bandwidth. The peak measured gain is 2.476 dBi at 2.75 GHz. The novel CSlSRR contributes to miniaturisation and enhancing the bandwidth of the antenna and also produces DNG material parameter response. As the antenna is compact, delivers enhanced bandwidth, RHCP, and decent gain over the band, the design is suitable for application in mobile electronic devices operating in the licensed and unlicensed bands of WLAN and WiMAX.

ACKNOWLEDGMENT

The authors would like to acknowledge the help of Prof (Dr) S Suganthi and Prof Shashi Kumar D of Department of Electronics and Communication Engineering, Christ University, Bengaluru, India for availing the facility at RF and Microwave research lab to carry out the antenna characterization.

REFERENCES

1. Randy, O. T. and Nasimuddin, "Circularly polarized slotted-ground microstrip antennas for radiofrequency identification reads," *Microw. Opt. Technol. Lett.*, Vol. 54, No. 10, 2304–2309, 2012.
2. Elftouh, H., N. Amar Touhami, M. Aghoutane, S. El Amrani, A. Tazón, and M. Boussouis, "Miniaturized microstrip patch antenna with defected ground structure," *Progress In Electromagnetics Research C*, Vol. 55, 25–33, 2014.
3. Jangid, K. G., A. Tiwari, V. Sharma, V. S. Kulhar, V. K. Saxena, and D. Bhatnagar, "Circular patch antenna with defected ground for UWB communication with WLAN band rejection," *Def. Sci. J.*, Vol. 66, No. 2, 162–167, 2016.

4. Khandelwal, M. K., B. K. Kanaujia, and S. Kumar, "Defected ground structure: Fundamentals, analysis, and applications in modern wireless trends," *International J. Antennas Propag.*, Vol. 2017, 1–21, 2017.
5. Arora, C., S. S. Pattnaik, and R. N. Baral, "SRR superstrate for gain and bandwidth enhancement of microstrip patch antenna array," *Progress In Electromagnetics Research B*, Vol. 76, 73–85, 2017.
6. Ali, T., S. Pathan, and R. C. Biradar, "A miniaturized circularly polarized coaxial fed superstrate slot antenna for L-band application," *Microw. Opt. Technol. Lett.*, Vol. 1, No. 6, 2018.
7. Arora, C., S. S. Pattnaik, and R. N. Baral, "SRR inspired microstrip patch antenna array," *Progress In Electromagnetics Research C*, Vol. 58, 89–96, 2015.
8. Patel, S. K., C. Argyropoulos, and Y. P. Kosta, "Broadband compact microstrip patch antenna design loaded by multiple split ring resonator superstrate and substrate," *Waves in Random and Complex Media*, Vol. 5030, 1–12, 2016.
9. Gao, X. J., T. Cai, and L. Zhu, "Enhancement of gain and directivity for microstrip antenna using negative permeability metamaterial," *AEU — Int. J. Electron. Commun.*, Vol. 70, No. 7, 880–885, 2016.
10. Dawar, P., A. De, and N. S. Raghava, "S-shaped metamaterial ultra-wideband directive patch antenna," *Radioelectron. Commun. Syst.*, Vol. 61, No. 9, 394–405, 2018.
11. Chaturvedi, D. and S. Raghavan, "SRR-loaded metamaterial-inspired electrically-small monopole antenna," *Progress In Electromagnetics Research C*, Vol. 81, 11–19, 2018.
12. Parvathy, A. R., V. G. Ajay, and T. Mathew, "Circularly polarized split ring resonator loaded slot antenna for RFID readers and WLAN applications," *Adv. Electromagn.*, Vol. 7, No. 5, 1–6, 2018.
13. Khalilpour, J. and M. Nosrati, "Micro-strip antenna with high bandwidth, cone pattern, circular polarization, and slit," *Electromagnetics*, Vol. 39, No. 1, 18–29, 2019.
14. Zhang, H., Y. Q. Li, X. Chen, Y. Q. Fu, and N. C. Yuan, "Design of circular polarisation microstrip patch antennas with complementary split ring resonator," *IET Microwaves, Antennas Propag.*, Vol. 3, No. 8, 1186–1190, 2009.
15. Zhang, H., Y. Li, X. Chen, Y. Fu, and N. Yuan, "Design of circular/dual-frequency linear polarization," *IEEE Trans. Antennas Propag.*, Vol. 57, No. 10, 3352–3355, 2009.
16. Singh, G., B. K. Kanaujia, V. K. Pandey, D. Gangwar, and S. Kumar, "Design of compact dual-band patch antenna loaded with D-shaped complementary split ring resonator," *Journal of Electromagnetic Waves and Applications*, Vol. 33, No. 16, 1–16, 2019.
17. Pandey, S. K., G. Prasad Pandey, and P. M. Sarun, "Circularly polarized micro-strip antenna with fractal trees loaded ground plane," *Electromagnetics*, Vol. 39, No. 7, 505–523, 2019.
18. Samson Daniel, R., R. Pandeeswari, and S. Raghavan, "Offset-fed complementary split ring resonators loaded monopole antenna for multiband operations," *AEU — Int. J. Electron. Commun.*, Vol. 78, 72–78, 2017.
19. Daniel, R. S., R. Pandeeswari, and S. Raghavan, "A miniaturized printed monopole antenna loaded with hexagonal complementary split ring resonators for multiband operations," *Int. J. RF Microw. Comput. Eng.*, Vol. 28, No. 7, 1–8, 2018.
20. Samanta, G. and S. R. Bhadra Chaudhuri, "Design of a compact CP antenna with enhanced bandwidth using a novel hexagonal ring based reactive impedance substrate," *Progress In Electromagnetics Research M*, Vol. 69, 115–125, 2018.
21. Catano-Ochoa, D., D. E. Senior, F. Lopez, and E. Reyes-Vera, "Performance analysis of a microstrip patch antenna loaded with an array of metamaterial resonators," *2016 IEEE International Symposium on Antennas and Propagation (APSURSI)*, 281–282, 2016.
22. Al-Bawri, S. S., H. H. Goh, S. Islam, and H. Y. Wong, "Compact ultra-wideband monopole antenna loaded with metamaterial," *Sensors*, Vol. 20, No. 3, 1–16, 2020.
23. Al-Bawri, S. S., S. Islam, H. Y. Wong, and M. F. Jamlos, "Bandwidth and gain enhancement of quad-band CPW-fed antenna for wireless applications," *Sensors*, Vol. 20, No. 2, 1–14, 2020.
24. Abdelrehim, A. A. A. and H. Ghafouri-shiraz, "High-performance terahertz antennas based on split ring resonator and thin wire," *Microw. Opt. Technol. Lett.*, Vol. 58, No. 2, 382–389, 2015.

25. Koutsoupidou, M., N. Uzunoglu, I. S. Karanasiou, and A. S. Description, "Antennas on metamaterial substrates as emitting components for THz biomedical imaging," *IEEE 12th International Conference on Bioinformatics & Bioengineering (BIBE)*, 11–13, Nov. 2012.
26. Ma, F., Y. Lin, X. Zhang, and C. Lee, "Tunable multiband terahertz metamaterials using a reconfigurable electric split-ring resonator array," *Light Sci. Appl.*, Vol. 3, 1–8, 2014.
27. Oliveira, J. G. D., E. N. M. G. Pinto, V. P. Silva Neto, and A. G. D'Assunção, "CSRR-based microwave sensor for dielectric materials characterization applied to soil water content determination," *Sensors*, Vol. 20, No. 2, 1–16, 2020.
28. Reyes-Vera, E., G. Acevedo-Osorio, M. Arias-Correa, and D. E. Senior, "A submersible printed sensor based on a monopole-coupled split ring resonator for permittivity characterization," *Sensors*, Vol. 19, No. 8, 1–12, 2019.
29. Hamidkhani, M. and F. Mohajeri, "Dual-band complementary split-ring resonator (CSRR) with high-quality factor and its applications in low phase noise oscillators and small multi-band diplexers and filters," *Progress In Electromagnetics Research M*, Vol. 52, 33–44, 2016.
30. Umair, H., et al., "A unique metamaterial inspired star-slot UWB antenna with soft surface ground," *Electromagnetics*, Vol. 40, No. 2, 152–163, 2020.
31. Krzysztofik, W. J. and T. N. Cao, "Metamaterials in application to improve antenna parameters," *Metamaterials and Metasurfaces*, 2018.
32. Pendry, J. B., A. J. Holden, D. J. Robbins, and W. J. Stewart, "Magnetism from conductors and enhanced nonlinear phenomena," *IEEE Trans. Microw. Theory Tech.*, Vol. 47, No. 11, 2075–2084, 1999.
33. Smith, D. R., S. Schultz, P. Markoš, and C. M. Soukoulis, "Determination of effective permittivity and permeability of metamaterials from reflection and transmission coefficients," *Phys. Rev. B*, Vol. 65, 1–5, 2002.
34. Smith, D., J. Gollub, J. J. Mock, and W. Padila, "Calculation and measurement of bianisotropy in a split ring resonator metamaterial," *J. Appl. Phys.*, Vol. 100, No. 3, 183–189, 2006.
35. Szabó, Z., G. Park, R. Hedge, and E. Li, "A unique extraction of metamaterial parameters based on Kramers-Kronig relationship," *IEEE Trans. Microw. Theory Tech.*, Vol. 58, No. 10, 2646–2653, 2010.
36. Smith, D. R., D. C. Vier, T. Koschny, and C. M. Soukoulis, "Electromagnetic parameter retrieval from inhomogeneous metamaterials," *Phys. Rev. E — Stat. Nonlinear, Soft Matter Phys.*, Vol. 71, No. 3, 1–11, 2005.
37. Baena, J. D., et al., "Equivalent-circuit models for split-ring resonators and complementary split-ring resonators coupled to planar transmission lines," *IEEE Trans. Microw. Theory Tech.*, Vol. 53, No. 4, 1451–1460, 2005.
38. Bilotti, F., A. Toscano, L. Vegni, K. Aydin, and K. B. Alici, "Equivalent-circuit models for the design of metamaterials based on artificial magnetic inclusions," *IEEE Trans. Microw. Theory Tech.*, Vol. 55, No. 12, 2865–2873, 2007.
39. Balanis, C. A., *Antenna Theory Analysis and Design*, 3rd Edition, Wiley-Interscience, 2005.